Experimental Techniques (2023) 47:989–1006
https://doi.org/10.1007/s40799-022-00604-2

RESEARCH PAPER

Experimental Dynamic Characterization of Both Surfaces of Structures using 3D Scanning Laser Doppler Vibrometer

Y. Chen[1] · **A. S. Escalera Mendoza**[1] · **D. T. Griffith**[1]

Received: 27 February 2022 / Accepted: 1 August 2022 / Published online: 24 August 2022

Abstract

Usually, only one surface or one side of 3D structures is measured in Scanning Laser Doppler Vibrometer (SLDV) tests due to test setup and instrumentation limitations. However, in this work, we demonstrate an approach to overcome these limitations while also using an SLDV that provides high spatial resolution measurement. In the case of a wind turbine blade, only one surface is typically measured. In most scenarios, only focusing on one surface of the blade is sufficient to characterize the dynamics of the global blade modes. However, as we show measurement of both surfaces offers valuable insights to explore both the global blade modes and the relative motions of the two surfaces of the blade. This work proposes and applies a new method of experimental modal testing on both surfaces of the wind turbine blade using a high spatial resolution 3D SLDV. The two surfaces of the wind turbine blade are scanned by the 3D SLDV respectively under the same global test coordinate system defined by several alignment objects. Then the two surfaces are stitched together to build the blade mode shapes of both surfaces. In the current testing, a total of over 1,500 points (4,500 response degrees of freedom for the 3D measurement) are scanned from both surfaces of the blade in a non-contact fashion to obtain the flap-wise, edge-wise, and torsional mode shapes of the blade. The orthogonality of the measured mode shapes, either one surface or both surfaces, is validated by the correlation tool, Modal Assurance Criterion (MAC). The effectiveness of the two-surface measurement is demonstrated by comparing the drive point Frequency Response Function and by correlating the mode shapes from the two surfaces. With the high spatial resolution 3D SLDV measurement, local panel modes of the wind turbine blade are observed from the mode shapes. Especially the panel breathing mode can only be revealed due to the two-surface measurement. This work also provides a useful reference for the wind turbine blade designers and researchers for design, structural analysis, and reliability study on the wind turbine blade. The two-surface measurement technique proposed in this work is demonstrated on a wind turbine blade, and it will also be applicable for other types of two-surface shell-type structures.

Keywords Wind Turbine Blade · 3D Scanning Laser Doppler Vibrometer (SLDV) · Modal Testing · Mode Shape · Modal Assurance Criterion (MAC) · Blade Panel Mode

Introduction

A wind turbine blade is one of the most complicated and essential elements of wind turbines. As blade length continuously grows, testing and modeling the wind turbine blade's modal characteristics to have an in-depth understanding of wind turbine blade dynamics is essential for the operation and service safety of a wind turbine [1].

What is the motivation to measure the mode shapes of both surfaces of structures, for example, wind turbine blades? In the existing literature, usually, due to the limitation of the test setup and instrumentation, only one surface of structure has been experimentally studied, and few works have addressed both surfaces of a structure. Specifically for the wind turbine blade, the configuration is hollow with a shear web or box spar supporting both surfaces [2]. There is a possibility that the two surfaces exhibit slightly different dynamic behavior, and there might be phase differences or relative displacement between the two surfaces. Although, for low-frequency mode shapes of a wind turbine blade, measuring one surface of the wind turbine blade is enough to capture the experimental

✉ Y. Chen
Yuanchang.Chen@UTDallas.edu

[1] Department of Mechanical Engineering, University of Texas at Dallas, Richardson, TX, USA

modal characteristics for global beam-type modes of a wind turbine blade. However, some high-order blade modes exhibit local panel modes, as shown in Reference [3, 4] via measurements with accelerometers placed on both sides of the blade. In some instances, having a better understanding of these local modes is necessary for blade damage detection and structural health monitoring [4–6]. A high-fidelity numerical model of the wind turbine blade, for example, a finite element model, can reveal these local panel modes [3]. But from an experimental perspective, both surfaces of a wind turbine blade have to be measured to experimentally characterize these local panel modes. Besides, with the mode shapes at both surfaces of the wind turbine blade measured, the mode shapes of both surfaces can be cross-correlated to validate the measured mode shapes, which is an additional benefit. In addition, for model validation, having the measured mode shapes at both surfaces of the wind turbine blade can improve understanding of blade dynamics and can also benefit the test-model correlation by providing extra experimental sensors for advanced model correlation to develop models that better capture localized effects and higher frequency dynamics. Extensively, this work can provide a general technique for capturing the dynamics of shell or plate structures where the relative motion of shells is important.

The finite element method can be used to develop the blade finite element model which can be useful to study the local panel modes because the finite element model has a large number of numerical sensors to address the blade geometry. However, developing a reliable blade finite element model requires a comprehensive knowledge of the blade's composite structural construction [7, 8]. In addition, the finite element model still needs experimental data to correlate to validate its accuracy.

To obtain the experimental mode shapes of a wind turbine blade, modal testing with accelerometers can be useful [9]. But due to the limited number of accelerometers and the data acquisition channels, and the concern of mass and cable loading, the measured blade mode shapes with accelerometers usually have a sparse spatial resolution. Though this is still useful for characterizing the low-order modes, it can have difficulties handling high-order modes and blade localized panel modes. Though the sensor expansion method [10–12] can increase the mode shape spatial resolution, it requires an additional algorithm and is also not applicable for the high-frequency range.

To directly acquire a large volume of experimental degrees of freedom (DOF) from the test blade, researchers have used either optical photogrammetry or Scanning Laser Doppler Vibrometer (SLDV) to measure the mode shape of one surface of the wind turbine blade. Lundstrom et al. [13] used high-speed stereophotogrammetry to extract shape information from wind turbine blade operating data. LeBlanc et al. [14] captured full-field displacement on the surface of a turbine blade with 3D DIC to detect damage. Baqersad et al. [15, 16] identified the full-field strain of a wind turbine blade with either stereophotogrammetry or 3D point tracking. Carr et al. [17] measured the full-field dynamic strain on wind turbine blades using digital image correlation. Wu et al. [18] monitored the wind turbine blades in operation using 3D digital image correlation. Khadka et al. [19] measured the mode shapes of rotating wind turbine blades with a flying drone. Luczak et al. [20] studied the test setup influence on the blade modes with the operational deflection shapes. Chen et al. [21–23] measured the 3D mode shapes from one surface of a wind turbine blade using 3D SLDV to study high-order mode shapes and mode coupling. However, only one surface of the wind turbine blades is of interest in these works, and both surfaces of a blade are not discussed.

Measurements on both sides of the blade with accelerometers were performed by Griffith et al. [3, 4]. However, the authors are not aware of any research on measuring both surfaces of the wind turbine blade using high-spatial resolution, non-contact 3D SLDV measurements. Blade modes including the panel modes can be captured from the modal test, but the measured mode shapes have sparse spatial resolution due to the limited number of accelerometers deployed on the blade. Witt et al. [24] measured three planar surfaces of a small size structure by using the 3D SLDV along with two mirrors. Yuan et al. [25] measured both surfaces of a small size plate by using the 3D SLDV and a mirror. This approach with the mirrors works well for small size structures and can ensure that the measurement points on both surfaces are measured simultaneously. However, this approach requires having a mirror and the size of the mirror needs to be large enough to reflect over the entire test structure. In addition, the relative position of the mirror to the test structure needs to be adjusted to obtain a good reflection image. Thus, this approach is not applicable to measure both surfaces for a large-size wind turbine blade.

In this work, to obtain the mode shapes on both surfaces, a mode shape stitching approach is developed and it is versatile for any 3D structure. Specifically, the mode shape of Surface 1 of a wind turbine blade is first measured with the Polytec 3D SLDV [26] under a modal shaker excitation. Then under exactly the same test setup, 3D SLDV is moved to the other side of the wind turbine blade to measure the mode shapes of Surface 2. The Surface 2 measurement follows the same coordinate system as the Surface 1 measurement. Under the same test coordinates defined by several alignment objects, the mode shapes of the Surface 1 are stitched together with the mode shapes of the Surface 2 to form the mode shapes on both surfaces, called Surface 1&2. The measured mode shapes of both blade surfaces can be used to identify the low and higher-order global flap-wise bending, edge-wise bending, and torsional modes as well as the local panel modes having

cross-sectional distortion. Thus, the technique presented here provides more information for global bending and torsional modes as well as new information regarding the relative motion and cross-section distortion.

The SLDV [27–29] uses three laser heads to measure the instantaneous vibration velocity in the direction of each laser beam. The three velocities measured along the direction of the laser beam are transformed into three global orthogonal directions via an orthogonal decomposition. After this mapping, the velocities at each laser scan point in three global orthogonal directions are obtained. SLDV is used as the mode shape measurement tool in this work because it can sweep over the blade surface to measure the vibration at as many points as desired, providing high spatial resolution mode shapes without sensor mass loading. The SLDV has the advantage of very sensitive measurement with a wide frequency range and can measure high-frequency modes. This is also useful for studying the local panel modes because these modes usually appear in the high-frequency range. The SLDV also has the benefit of not requiring any speckling of the test structure surface before the test, which is required for full-field measurement techniques, for instance, DIC, where a dot pattern or targets are required.

The outline of the paper is as follows. Section 2 develops the theory behind the two-surface mode shape measurement technique. Section 3 introduces the testbed, including the blade and the test platform. Section 4 presents the 3D SLDV test setup. Section 5 shows the modal testing result of Surface 1, Surface 2, and Surface 1&2, respectively. Section 6 has some discussion of several relevant topics. Section 7 concludes the work.

Theory

The theory related to the mode shapes measurement and validation on both surfaces of a structure is discussed in this section.

Stitching Method

A stitching method is used in this work to combine the mode shapes of two surfaces together. To show its versatility, a simple beam is used as an example here to illustrate the stitching technique, as shown in Fig. 1.

STEP 1

3D SLDV is instrumented on one side of the structure. The global test coordinate system is defined by several alignment objects beyond the testbed. The alignment objects are used for the geometry scan unit of 3D SLDV to perform 3D alignment and define the global test coordinate system. The alignment objects are positioned so that they are visible for the 3D SLDV instrumented on either side of the structure. After the global test coordinate system is defined, the mode shapes of Surface 1 of the structure can be measured with the 3D SLDV.

STEP 2

After the mode shapes of Surface 1 of the structure are measured, the 3D SLDV is moved to the other side of the structure. It should be noted that, in this 3D SLDV transition, the testbed and the alignment objects should not be moved. The test coordinate system of the Surface 2 is defined to be exactly the same as the test coordinate system of Surface 1 by performing the 3D alignment on the same alignment objects. After the test coordinate system is defined for Surface 2, the mode shapes of the Surface 2 can be measured.

STEP 3

Because the mode shapes of both surfaces of the structure are measured in the same global coordinate system with the

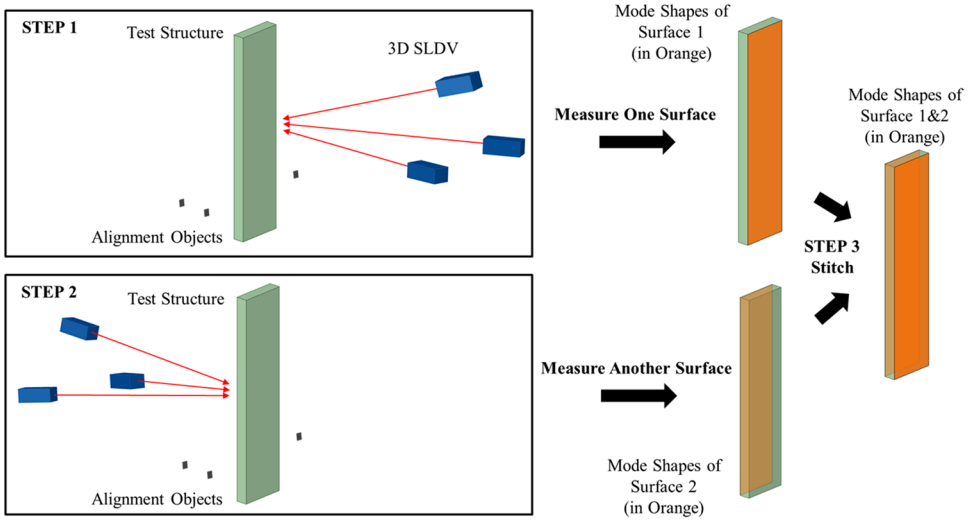

Fig. 1 Process of Mode Shape Stitching of the Two Surfaces

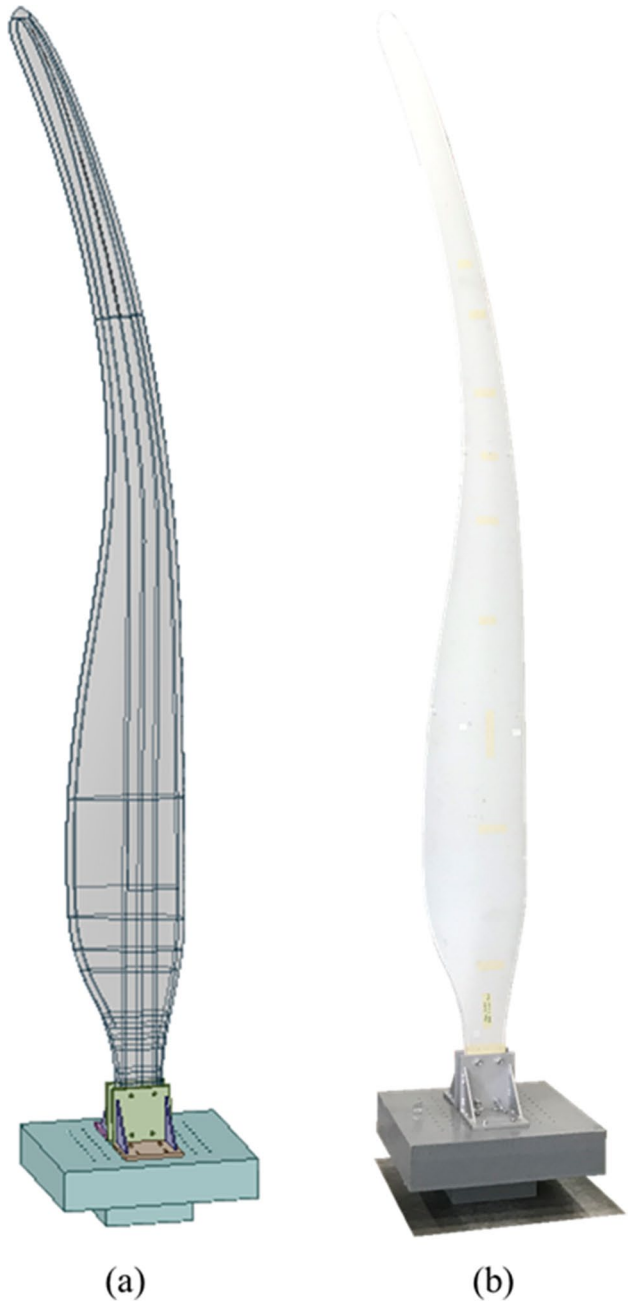

Fig. 2 Testbed. (**a**) CAD Geometry; (**b**) Photo

assistance of the alignment objects, the mode shapes of the two surfaces can be stitched together to build the structural mode shapes on both surfaces with the combined surfaces again denoted as Surface 1&2.

Modal Assurance Criterion (MAC)

The MAC [30] is a tool for quantifying the correlation between two mode shape sets at all degrees of freedom. The MAC is written as:

$$MAC = \frac{\left(U^T V\right)^2}{\left(U^T U\right)\left(V^T V\right)} \tag{1}$$

where U and V represent two same dimension mode shape sets having m mode shapes ($m \geq 1$). When $U = V$, MAC is called AutoMAC, which represents the auto-correlation of the mode shape set. AutoMAC is useful for examining the orthogonality of the mode shapes within a mode shape set. When $U \neq V$, MAC is called CrossMAC, which represents the cross-correlation between the two mode shape sets. CrossMAC is useful for checking the similarity of the mode shapes between two mode shape sets. The MAC values close to 1.0 indicate strong similarity, whereas values close to 0.0 indicate minimal or no similarity.

Testbed

In this work, there is interest in studying the mode shapes of both surfaces of the wind turbine blade. Hence, a test platform [31] is designed and manufactured to hold the blade vertically, as shown in Fig. 2. The exploded view of the testbed is shown in Fig. 3. The testbed includes one wind turbine blade and one test platform. The test platform is a seismic mass made of steel that rests on the ground and holds the wind turbine blade vertically with the aid of two fixture clamps (each one of each wide and flat side of the blade root), as shown in Fig. 3.

The dense and highly rigid testing platform fixes the root of the blade such that it behaves like a cantilever beam. The advantage of using this test stand is that it places the blade

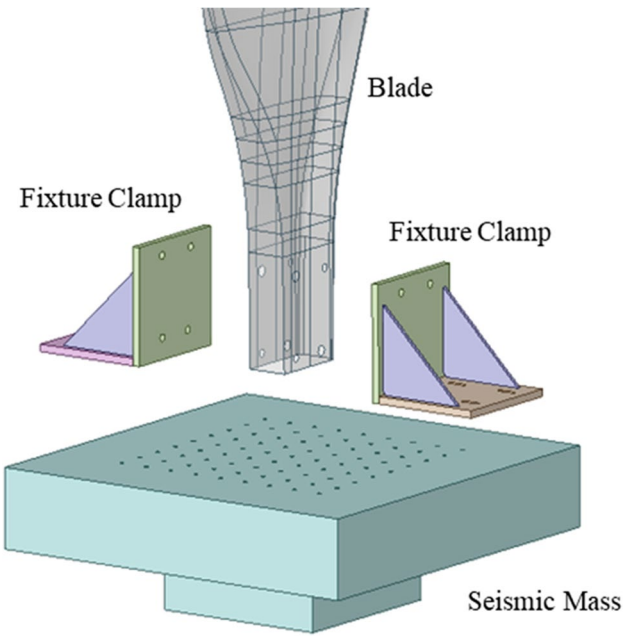

Fig. 3 Exploded View of the Test Platform

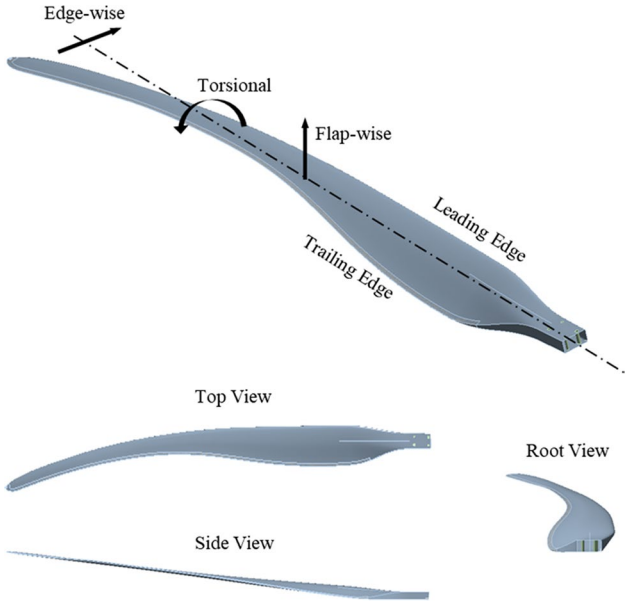

Fig. 4 CAD Geometry of Single Blade

vertically and allows the 3D SLDV to scan one side of the blade surface in one test. This can be achieved by setting up the 3D SLDV to be far enough away to be able to scan the entire blade, but still maintain a strong laser return signal. A more detailed description of the test blade and the test platform is provided next.

Wind Turbine Blade

The wind turbine blade shown in Fig. 4 is designed and manufactured to operate in an 8-kilowatt stall regulated machine that is onshore and upwind. The blade weighs 17.6 kg (38.8 pounds). The blade is 4.2 m long, it is designed with the SG6040 airfoil and has varying structural properties along its length and chord that are driven by the blade geometry (non-constant chord, twist, pre-bend, and sweep) as well as by the multiple materials (that vary in quantity and location) used in its construction. The flap-wise, edge-wise, and torsional terms, used to classify the different mode shapes, correspond to the directions indicated in Fig. 4.

Figure 5 shows the location of the different materials along the cross-section at the 0.9 m span location (along the blade length). The quantity (i.e., thickness) of these varies from the root of the blade to the tip making the whole wind turbine blade a geometrically complex composite structure with anisotropic properties.

Test Platform

A test platform is placed on the ground and is necessary to function as a platform to conduct tests on the wind turbine blades, as shown in Fig. 3. The test platform contains three parts, a large piece of mass, called seismic mass, and two fixture clamps, which are described below.

Seismic Mass

The seismic mass holds the wind turbine blade and fixture clamps so that the wind turbine blade is centered as shown in Fig. 2. The seismic mass is composed of two A36 Steel plates welded together and in total weigh approximately 597 kg (1,316 pounds). The top surface of seismic mass has a 9×9 bolt pattern (81 holes in total) of M8 bolts. The grid pattern has 50.8 mm (2 inches) even spacing with a hole depth of 38.1 mm (1.5 inches). This grid pattern is designed to allow for future use of the seismic mass to support different fixtures and different test objects.

Fixture Clamp

The fixture clamp is made from AISI 1045 steel plates that are welded together to form rigid support of the blade root. One fixture clamp weighs about 9.1 kg (20 pounds). Two fixture clamps are bolted to the seismic mass with 8 bolts (size M8-1.0 class 8.8 medium carbon steel) and the blade is attached to the two fixture clamps using 4 bolts and nuts (size M12-1.25 class 8.8 medium carbon steel). Washers are

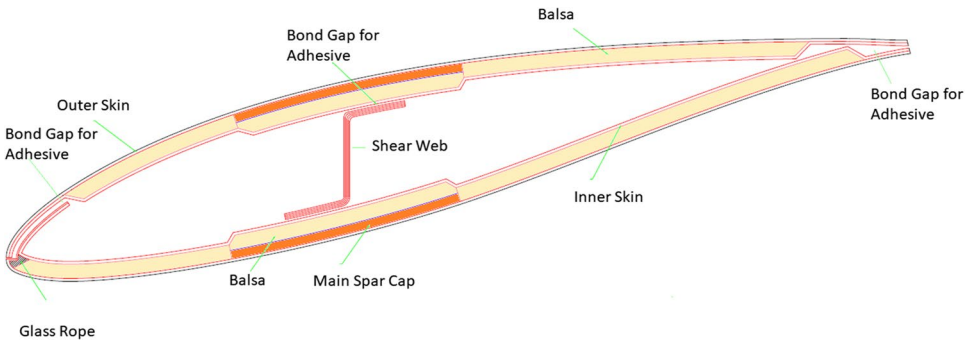

Fig. 5 Blade Cross-Section at Blade Span Station 0.9 m from the Blade Root

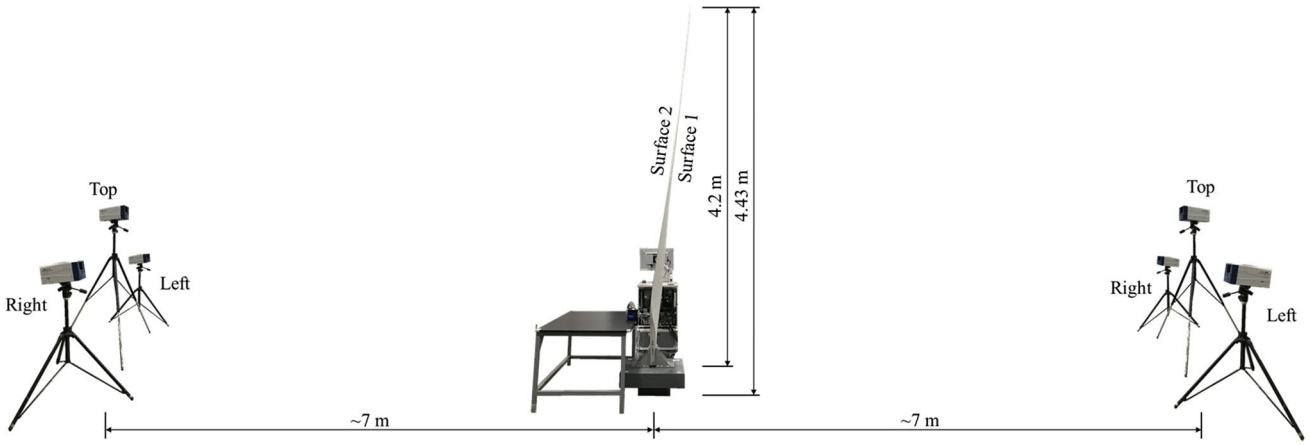

Fig. 6 3D SLDV Test Overview

Fig. 7 3D SLDV Test Setup

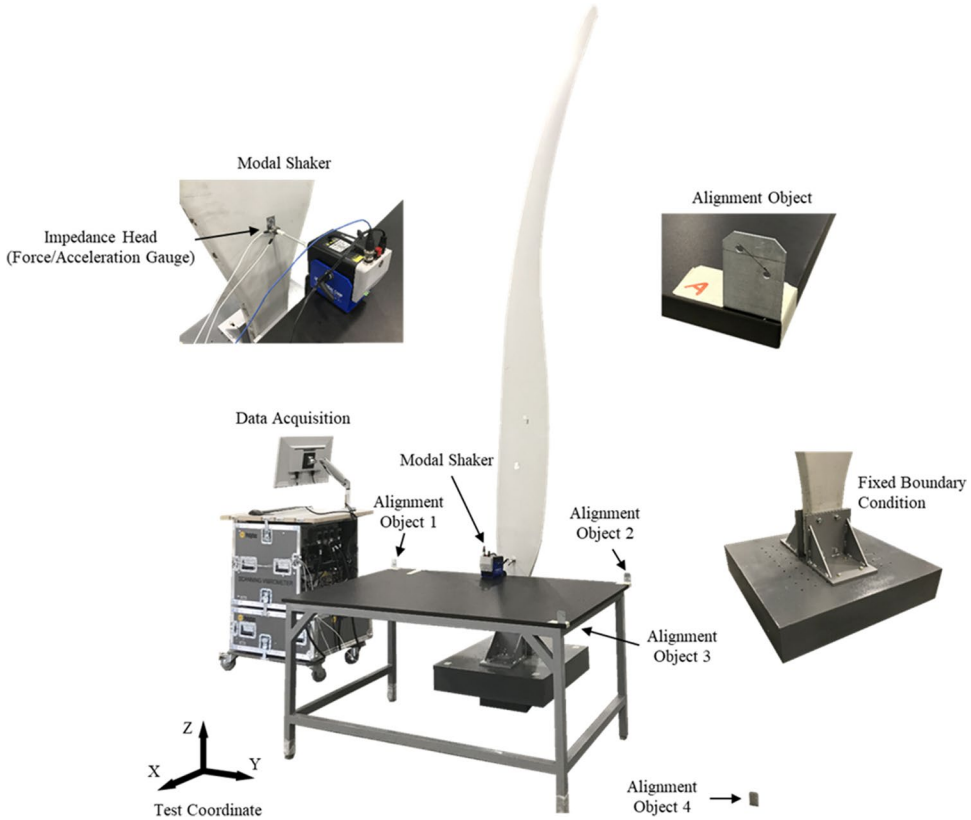

also placed between the bolts and the fixture clamps for both the M8 and M12 bolts to help distribute the clamping load.

Since the seismic mass is much heavier than the blade and the fixture clamp provides rigid support for the blade root, the accelerometer test on the blade and seismic mass (test does not show here) indicate that the seismic mass placed on the ground does not exhibit rigid body modes. The seismic mass can be regarded to have a firm attachment to the ground. In addition, nonlinearity has not been found, and the blade sitting on the seismic mass system can be regarded as linear. Overall, the boundary condition of the blade sitting on the seismic mass is a cantilever.

Table 1 Test Instruments

Test Instruments	Vendor	Type
3D SLDV	Polytec, Inc	PSV-500-3D
Shaker	Modal Shop, Inc	K2004E01

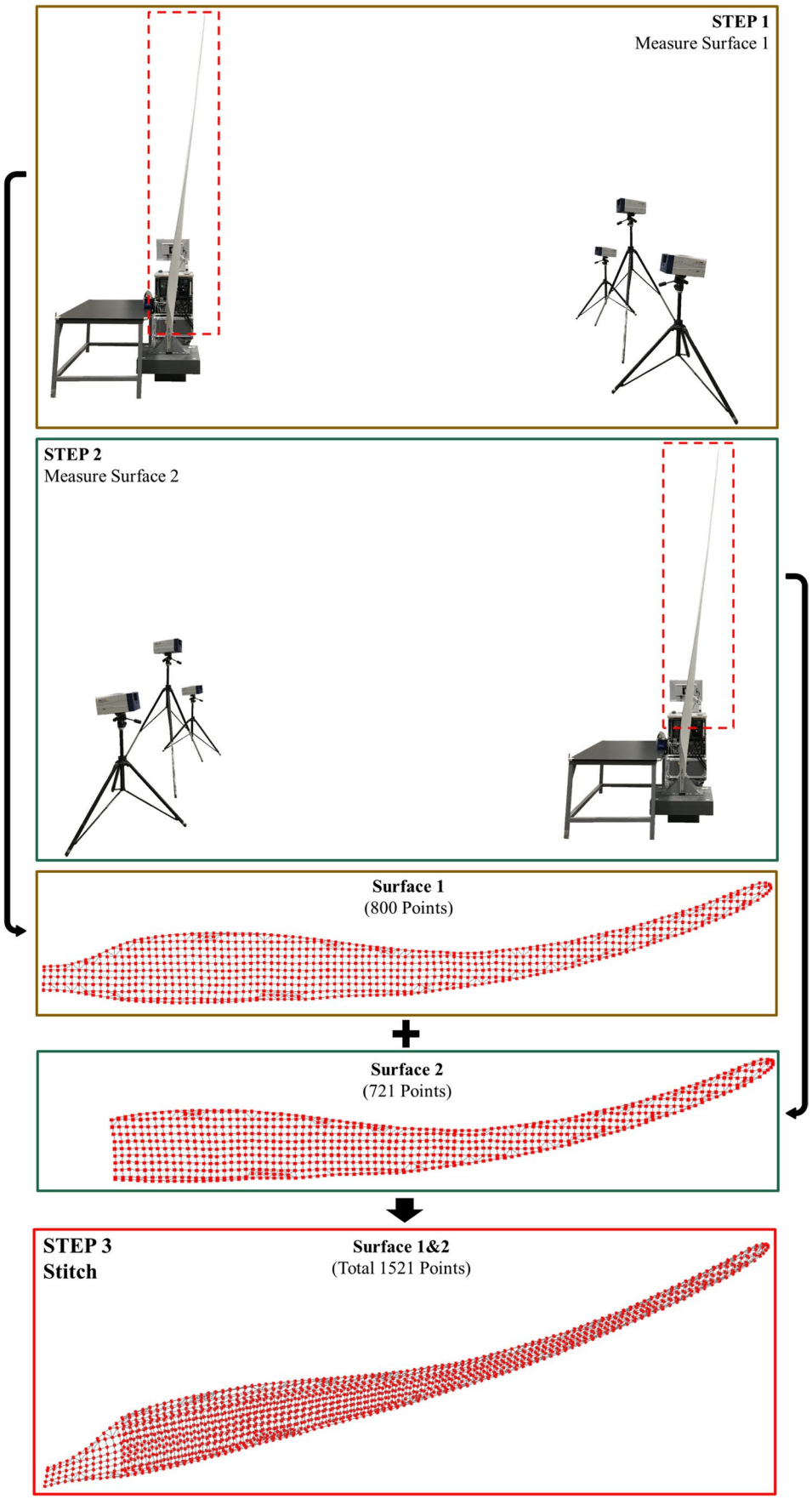

Fig. 8 3D SLDV Test Steps and Scanned Points

Table 2 3D SLDV Test Parameters

Test Parameters	Value
Shaker Excitation	Pseudo Random
Surface 1	800 Points
Surface 2	721 Points
Frequency Bandwidth	312.5 Hz
Frequency Lines	3200
Frequency Resolution	0.1 Hz
Time for Each Average	10.24 s
Window	No Window
FRF Average	3

Test Setup

The test strategy of mode shapes measurement on both surfaces of the wind turbine blade is shown in Fig. 6. The height of the vertical blade is 4.2 m and the total height of the blade on the test platform is 4.43 m. First, the 3D SLDV is instrumented on one side of the blade to measure the mode shapes of Surface 1. The 3D SLDV is setup to have enough spatial distance away from the blade so that the laser beam shooting from the three aligned laser heads can cover the entire blade up to the blade tip down to the blade root. After the mode shapes of Surface 1 of the blade are measured, the 3D SLDV is moved to the other side of the blade. 3D SLDV is the only equipment that is transited, and all the test items except the 3D SLDV should not be moved. Then, the mode shapes of the Surface 2 of the blade are measured. Finally, the mode shapes of both surfaces are stitched together to build the mode shapes of the combined surface denoted as Surface 1&2.

The test setup is shown in Fig. 7, and the test instruments used are listed in Table 1. The root of the blade is bolted firmly to the test platform with four bolts, as shown on the right side of Fig. 7. A modal shaker, fixed to a large heavy table, is attached to the Surface 2 of the blade via an impedance head, as shown in the top left corner of Fig. 7. The impedance head has a force/acceleration gauge built-in to record the force and acceleration applied to the blade. A modal shaker is orientated in a skewed fashion to provide adequate energy input for both flap-wise and edge-wise directions.

There are four independent alignment objects used to define the global test coordinate system, as shown in the top right corner of Fig. 7. The reason for using these independent alignment objects instead of using the points on the testbed is that these alignment objects should be visible for the 3D SLDV instrumented on either side of the blade. Another requirement for these alignment objects is that they should be thin. In this matter, no matter which side of the blade the 3D SLDV locates, the 3D coordinate read from the geometry scan unit of 3D SLDV is regarded to be the same. When defining the test coordinate system for the measurement of Surface 1 of the blade, the geometry laser from the geometry scan unit of 3D SLDV focuses on one location on the alignment objects, indicated by the cross on the alignment object, to perform the 3D alignment and the 3D coordinates of this location are recorded. This 3D coordinate system is also used as the global test coordinate system for the measurement of Surface 2. When performing a 3D alignment after the 3D SLDV is transited to the other side of the blade, the geometry laser from the geometry scan unit of 3D SLDV focuses on the same location of the alignment objects but on the opposite side. The global 3D coordinates defined from the previous 3D alignment are used to define the test coordinate system. Alignment Object 1 defines the origin of the global test coordinate system, which is zero. The Alignment Object 2 defines the + Y axis. The Alignment Object 3 defines the X–Y plane. Alignment Object 4 defines an alignment point outside of the X–Y plane. The alignment objects should have some spatial distance from each other to avoid crowdedness. High alignment quality is required to ensure that the three laser beams are well focused on the scan point.

Under the shaker excitation, the velocity response in three dimensions at every scan point is measured by the three aligned SLDV heads, one at a time. This blade surface is a good laser reflector, and the laser signal acquisition has a reasonable laser reflection rate, so there is no need to stick reflective tape at the laser scan points to increase the laser reflection. With three Frequency Response Function (FRF) averages for each scan point, FRF at each scan point is obtained from the measured input shaker force and acceleration, and the measured output velocity response at each scan point.

To obtain blade mode shapes with high spatial resolution, a large volume of scan points is defined for the mode shape measurement, as shown in Fig. 8. For the Surface 1 measurement, the laser beams of 3D SLDV can reach up to the blade tip and down to the blade root, as shown by the red dashed box in Step 1 in Fig. 8. An 800-Point scan grid is defined for Surface 1. The same scan grid is applied on Surface 2. When measuring Surface 2, the shaker and the table should remain unmoved. Because of this, the shaker and the table block the laser beam's path, the scan points at the root of the Surface 2 can not be reached by the laser beams of 3D SLDV, as shown by the red dashed box in Step 2 in Fig. 8. The scan points at the root of the Surface 2 are removed from the 800-Point scan grid, and a 721-Point scan grid is defined for Surface 2.

The same shaker excitation is used when scanning Surface 1 and Surface 2. As described above, Surface 1 and Surface 2 are scanned separately, but the two surfaces are scanned under the same global test coordinate system

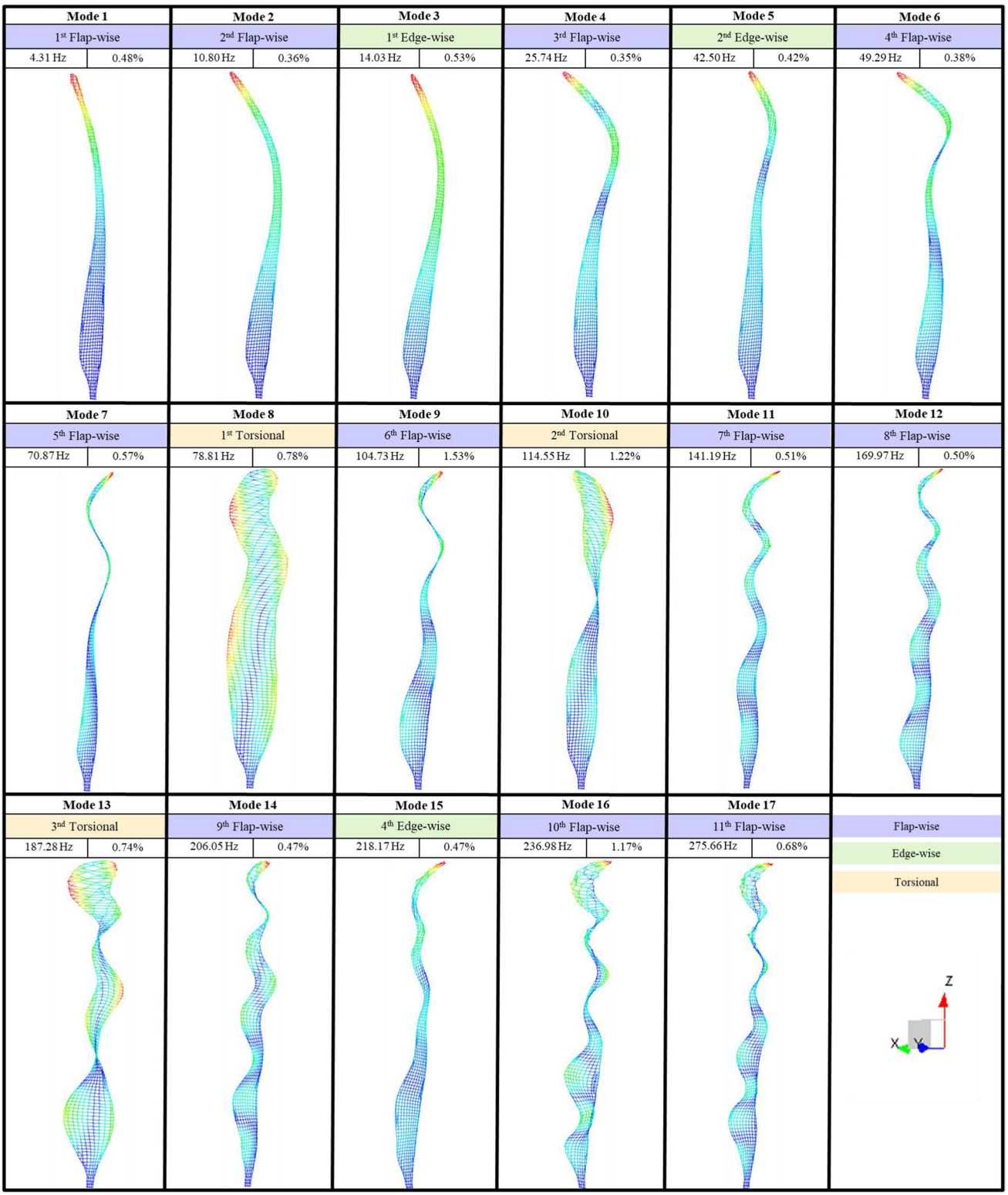

Fig. 9 Modal Parameters of the Surface 1

defined by the alignment objects. Then, the geometry of the two surfaces is stitched together to form the whole blade's scan geometry, as shown in Step 3 in Fig. 8. There is a total of 1,521 scan points defined on both surfaces. Each scan point has 3 DOF responses measured. Thus, there is a total of 4,563 DOF measured from both surfaces.

90%-100%	70%-90%		Surface 1															
50%-70%	0-30%		Mode 1	Mode 2	Mode 3	Mode 4	Mode 5	Mode 6	Mode 7	Mode 8	Mode 9	Mode 10	Mode 11	Mode 12	Mode 13	Mode 14	Mode 15	Mode 16	Mode 17
		MAC	4.31 Hz	10.8 Hz	14.03 Hz	25.74 Hz	42.5 Hz	49.29 Hz	70.87 Hz	78.81 Hz	104.73 Hz	114.55 Hz	141.19 Hz	169.97 Hz	187.28 Hz	206.05 Hz	218.17 Hz	236.98 Hz	275.66 Hz
Surface 1	Mode 1	4.31 Hz	100%	4%	2%	2%	1%	1%	3%	0%	3%	2%	2%	2%	0%	1%	1%	0%	1%
	Mode 2	10.8 Hz	4%	100%	0%	8%	0%	3%	2%	0%	2%	0%	2%	2%	0%	2%	2%	0%	1%
	Mode 3	14.03 Hz	2%	0%	100%	1%	6%	0%	0%	1%	1%	0%	0%	1%	0%	2%	0%	0%	0%
	Mode 4	25.74 Hz	2%	8%	1%	100%	3%	9%	3%	0%	1%	0%	3%	4%	0%	2%	3%	1%	2%
	Mode 5	42.5 Hz	1%	0%	6%	3%	100%	2%	4%	0%	2%	0%	0%	1%	1%	1%	0%	1%	1%
	Mode 6	49.29 Hz	1%	3%	0%	9%	2%	100%	5%	1%	1%	0%	4%	2%	1%	2%	3%	0%	1%
	Mode 7	70.87 Hz	3%	2%	0%	3%	4%	5%	100%	0%	7%	1%	4%	3%	0%	2%	2%	2%	3%
	Mode 8	78.81 Hz	0%	0%	1%	0%	0%	1%	0%	100%	0%	5%	0%	0%	0%	0%	0%	0%	0%
	Mode 9	104.73 Hz	3%	2%	1%	1%	2%	1%	7%	0%	100%	1%	6%	4%	0%	3%	0%	0%	3%
	Mode 10	114.55 Hz	2%	0%	0%	0%	0%	0%	1%	5%	1%	100%	1%	1%	4%	0%	0%	0%	0%
	Mode 11	141.19 Hz	2%	2%	0%	3%	0%	4%	4%	0%	6%	1%	100%	8%	0%	2%	8%	4%	2%
	Mode 12	169.97 Hz	2%	2%	1%	4%	1%	2%	3%	0%	4%	1%	8%	100%	1%	7%	1%	1%	4%
	Mode 13	187.28 Hz	0%	0%	0%	0%	1%	1%	0%	0%	0%	4%	0%	1%	100%	0%	0%	3%	2%
	Mode 14	206.05 Hz	1%	2%	2%	2%	1%	2%	2%	0%	3%	0%	2%	7%	0%	100%	4%	1%	1%
	Mode 15	218.17 Hz	1%	2%	0%	3%	0%	3%	2%	0%	0%	0%	8%	1%	0%	4%	100%	2%	2%
	Mode 16	236.98 Hz	0%	0%	0%	1%	1%	0%	2%	0%	0%	0%	4%	1%	3%	1%	2%	100%	5%
	Mode 17	275.66 Hz	1%	1%	0%	2%	1%	1%	3%	0%	3%	0%	2%	4%	2%	1%	2%	5%	100%

Fig. 10 AutoMAC of the Mode Shapes of the Surface 1

The test parameters of the 3D SLDV measurement are shown in Table 2. Pseudo random is used as the shaker input signal. Thus, no window is needed for the data acquisition. The frequency bandwidth is selected up to 312.5 Hz to capture the local panel modes because the local panel modes are at a higher frequency compared to the lowest blade mode at around 4 Hz [21]. The frequency resolution is determined as fine as 0.1 Hz to provide a detailed frequency resolution for identifying the mode frequency. The FRF average is set as three because the coherence of the FRF measurement would be stable in three averages.

Overall, the coordinates of the scan points of the two surfaces are defined under the same global coordinate system via the same alignment objects. The FRFs and the geometry coordinates of the scan points at Surface 1 are first measured, then measured for Surface 2. Surface 1 and Surface 2 is stitched by combing the FRFs and the geometry coordinates of Surface 1 and Surface 2 in the Polytec software [26] to generate Surface 1&2.

Test Results

The FRFs of 800 scan points at Surface 1 (2,400 FRFs) along with the geometry of 800 scan points are imported into Simcenter TestLab [32]. The PolyMax algorithm [32] is used to estimate the modal parameters, including frequency, damping, and mode shapes. Then, the FRFs of 721 scan points at Surface 2 (2,163 FRFs) along with the geometry of 721 scan points are imported into Simcenter TestLab separately and are processed to obtain the frequency, damping, and mode shapes of Surface 2. Finally, all FRFs (4,563 FRFs) and the geometry of all scan points (1,521 points) are processed together to obtain the modal parameters of both surfaces.

In this section, the modal parameters results are shown for Surface 1, Surface 2, and Surface 1&2, respectively, in three sub-sections. And all modes below 300 Hz are included. Different colors classify the type of mode. The primary deformation type of the modes determines the color. For example, if the mode's primary deformation is flap-wise, the color would be marked as blue; if the mode's primary deformation is torsional, it would be marked as yellow. In addition, the AutoMAC is performed to correlate the mode shape set to themselves. This is to validate the orthogonality of the measured mode shapes to each other in the mode shape set.

Surface 1 Measurement

The modal parameters below 300 Hz measured from the blade Surface 1 are shown in Fig. 9. As shown in Fig. 9, the mode shapes of the high-order modes have a more complex curvature than the low-order mode shapes. Because of the three-dimensional response measurement, the flap-wise, edge-wise, and torsional types of deformation are shown in the modes. The mode primary deformation and the corresponding mode order are marked on top of each mode. Also, with a large number of points measurement capability, the mode shapes can be better visualized, especially for the high-order mode shapes with complex curvature.

If the identified mode shapes are noisy, a Gaussian spatial filter in Polytec software [26] is available to smooth and polish the measured mode shapes. In this work, Mode 1 has a noisy mode shape from blade tip down 2 m, and its mode shape quality is improved by using the spatial filter as a low-pass smoothing function. In addition, this spatial filter is also useful for improving the stitching quality of the two surfaces, which is discussed in detail in Sect. 5.3. The MAC is then calculated on the Surface 1 mode set, as shown in Fig. 10. In this figure, the off-diagonal terms of the MAC table are below 10%. This fact shows that the

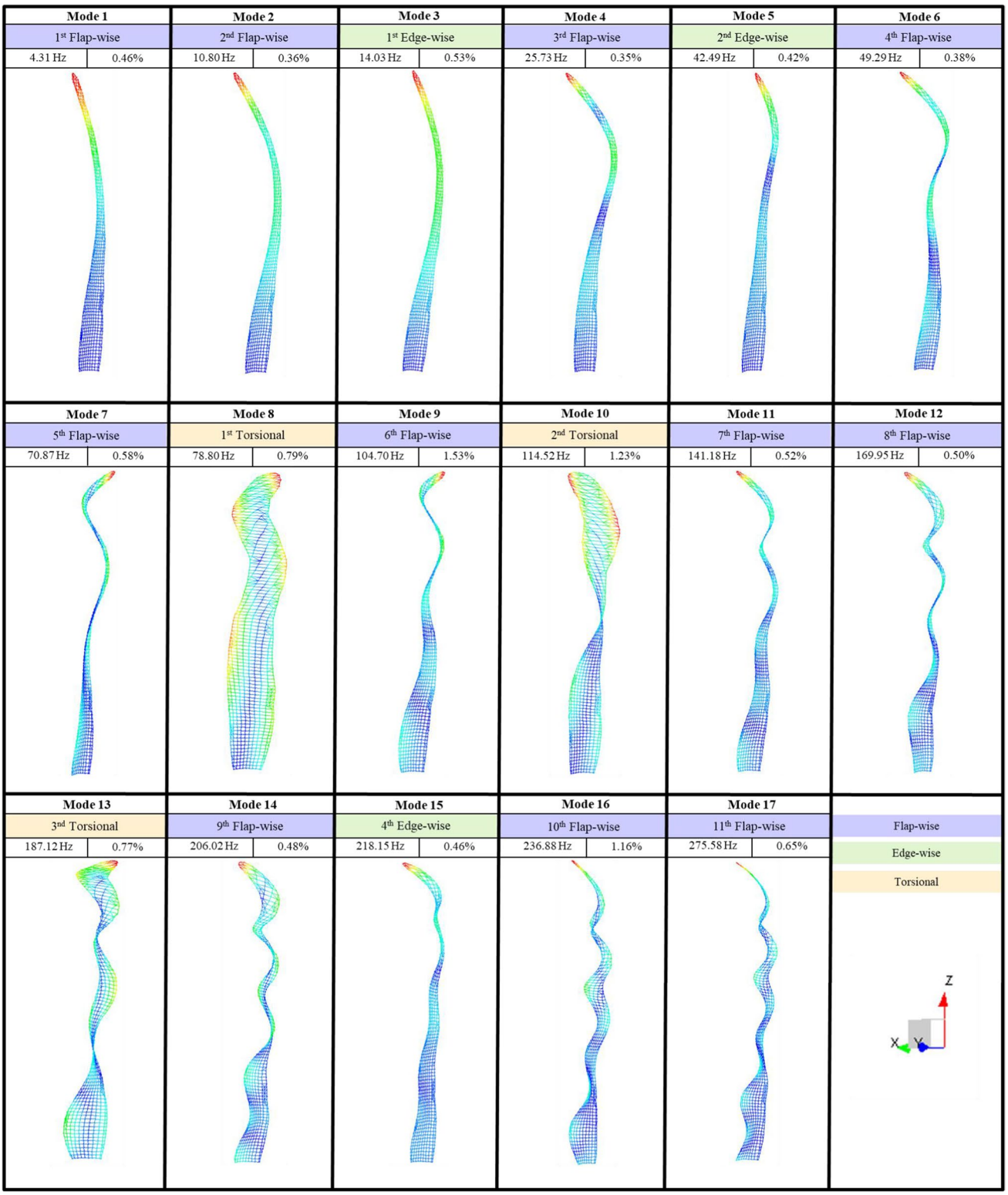

Fig. 11 Modal Parameters of the Surface 2

measured mode shapes of the Surface 1 mode set have high orthogonality, which indicates an effective mode shapes measurement for the Surface 1 of the blade.

Surface 2 Measurement

Similar to Surface 1, the modal parameters of the Surface 2

90%-100%	70%-90%		Surface 2															
50%-70%	0-30%		Mode 1	Mode 2	Mode 3	Mode 4	Mode 5	Mode 6	Mode 7	Mode 8	Mode 9	Mode 10	Mode 11	Mode 12	Mode 13	Mode 14	Mode 15	Mode 16	Mode 17
		MAC	4.31 Hz	10.8 Hz	14.03 Hz	25.73 Hz	42.49 Hz	49.28 Hz	70.87 Hz	78.79 Hz	104.68 Hz	114.47 Hz	141.17 Hz	169.92 Hz	186.99 Hz	205.99 Hz	218.12 Hz	236.73 Hz	275.54 Hz
Surface 2	Mode 1	4.31 Hz	100%	5%	2%	2%	1%	1%	3%	0%	2%	0%	3%	2%	2%	1%	2%	3%	3%
	Mode 2	10.8 Hz	5%	100%	0%	10%	0%	4%	2%	3%	3%	0%	3%	3%	0%	2%	3%	3%	5%
	Mode 3	14.03 Hz	2%	0%	100%	1%	7%	0%	0%	1%	0%	0%	1%	1%	0%	1%	0%	1%	1%
	Mode 4	25.73 Hz	2%	10%	1%	100%	3%	10%	5%	0%	3%	2%	5%	4%	3%	4%	4%	5%	4%
	Mode 5	42.49 Hz	1%	0%	7%	3%	100%	1%	3%	4%	3%	0%	1%	2%	2%	1%	0%	4%	4%
	Mode 6	49.28 Hz	1%	4%	0%	10%	1%	100%	6%	3%	2%	0%	7%	3%	2%	1%	5%	4%	6%
	Mode 7	70.87 Hz	3%	2%	0%	5%	3%	6%	100%	0%	11%	0%	6%	6%	1%	3%	3%	6%	8%
	Mode 8	78.79 Hz	0%	3%	1%	0%	4%	3%	0%	100%	1%	8%	2%	2%	0%	1%	1%	2%	2%
	Mode 9	104.68 Hz	2%	3%	0%	3%	3%	2%	11%	1%	100%	0%	13%	5%	4%	6%	2%	6%	7%
	Mode 10	114.47 Hz	0%	0%	0%	2%	0%	0%	0%	8%	0%	100%	3%	0%	6%	0%	2%	2%	2%
	Mode 11	141.17 Hz	3%	3%	1%	5%	1%	7%	6%	2%	13%	3%	100%	17%	1%	2%	12%	6%	10%
	Mode 12	169.92 Hz	2%	3%	1%	4%	2%	3%	6%	2%	5%	0%	17%	100%	8%	15%	5%	7%	11%
	Mode 13	186.99 Hz	2%	0%	0%	3%	2%	2%	1%	0%	4%	6%	1%	8%	100%	2%	1%	13%	7%
	Mode 14	205.99 Hz	1%	2%	1%	4%	1%	1%	3%	1%	6%	0%	2%	15%	2%	100%	7%	7%	3%
	Mode 15	218.12 Hz	2%	3%	0%	4%	0%	5%	3%	1%	2%	2%	12%	5%	1%	7%	100%	5%	6%
	Mode 16	236.73 Hz	3%	3%	1%	5%	4%	4%	6%	2%	6%	2%	6%	7%	13%	7%	5%	100%	25%
	Mode 17	275.54 Hz	3%	5%	1%	4%	4%	6%	8%	2%	7%	2%	10%	11%	7%	3%	6%	25%	100%

Fig. 12 AutoMAC of the Mode Shapes of the Surface 2

are measured and are shown in Fig. 11. As shown in Fig. 11, the Surface 2 modes have similar mode shapes to the Surface 1 modes, which is as expected. The area near the root of the Surface 2 is not measured due to the inaccessibility of the laser beams of 3D SLDV to this area where the shaker is mounted.

The MAC is then calculated on the Surface 2 mode set, as shown in Fig. 12. The off-diagonal terms of the MAC table are below 25%. The mode shapes of the Surface 2 also have high orthogonality.

Surface 1&2 Stitching

The FRF and geometry coordinates of Surface 1 and Surface 2 are processed together in PolyMax, as shown in Fig. 13. Also, to provide an orthogonal view of the obtained mode shapes, several primary modes in their corresponding main plane are plotted in Fig. 14.

The FRF and geometry coordinates of Surface 1 and Surface 2 are processed together to yield the mode shapes on Surface 1&2. For the mode shapes of Surface 1&2 in Fig. 13, Surface 1 is generally well overlaid with Surface 2. However, there is a mode shape difference at the blade tip between Surface 1 and Surface 2, which occurs more frequently in high-order modes. This is due to the slight test coordinate difference between Surface 1 and Surface 2. The test coordinate system of the Surface 1 is first defined when measuring Surface 1, then Surface 2 is designed to follow the same test coordinate system as Surface 1. However, when defining the test coordinate of Surface 2, which is also the 3D alignment, the geometry laser has to be manually moved to focus on the same 3D alignment locations. Because of this manual 3D alignment process for Surface 2, the test coordinate of the Surface 2 would not be exactly the same as Surface 1. This contributes to the slight mode shape difference between the two surfaces. In addition, the blade tip has larger deformation than the other parts of the blade, so even tiny test coordinate differences between the two surfaces can contribute to the mode shape difference. Same as previous, the AutoMAC is calculated on the mode set of Surface 1&2, as shown in Fig. 15. The off-diagonal terms of the MAC table are not higher than 10%. The mode shapes of the Surface 1&2 are also orthogonal to each other.

Discussion

Some items are discussed in this section related to the mode shapes of both surfaces.

Two-Surface Stitching Quality

To obtain the effective stitching of the mode shapes of the two surfaces, three requirements must be met. First, the test coordinate system of the Surface 2 should follow the same test coordinate system of Surface 1. This is also discussed in the previous section. For the measurement in this work, the authors have done their best to align the test coordinate system of Surface 2 to Surface 1 using thin reference objects placed on stable supports. Second, the shaker excitation force when measuring the two surfaces, including the force amplitude and force signal, should be the same. This requirement is met by maintaining the same shaker generator setting when measuring the two surfaces. Third, the data measured from the same point from the two

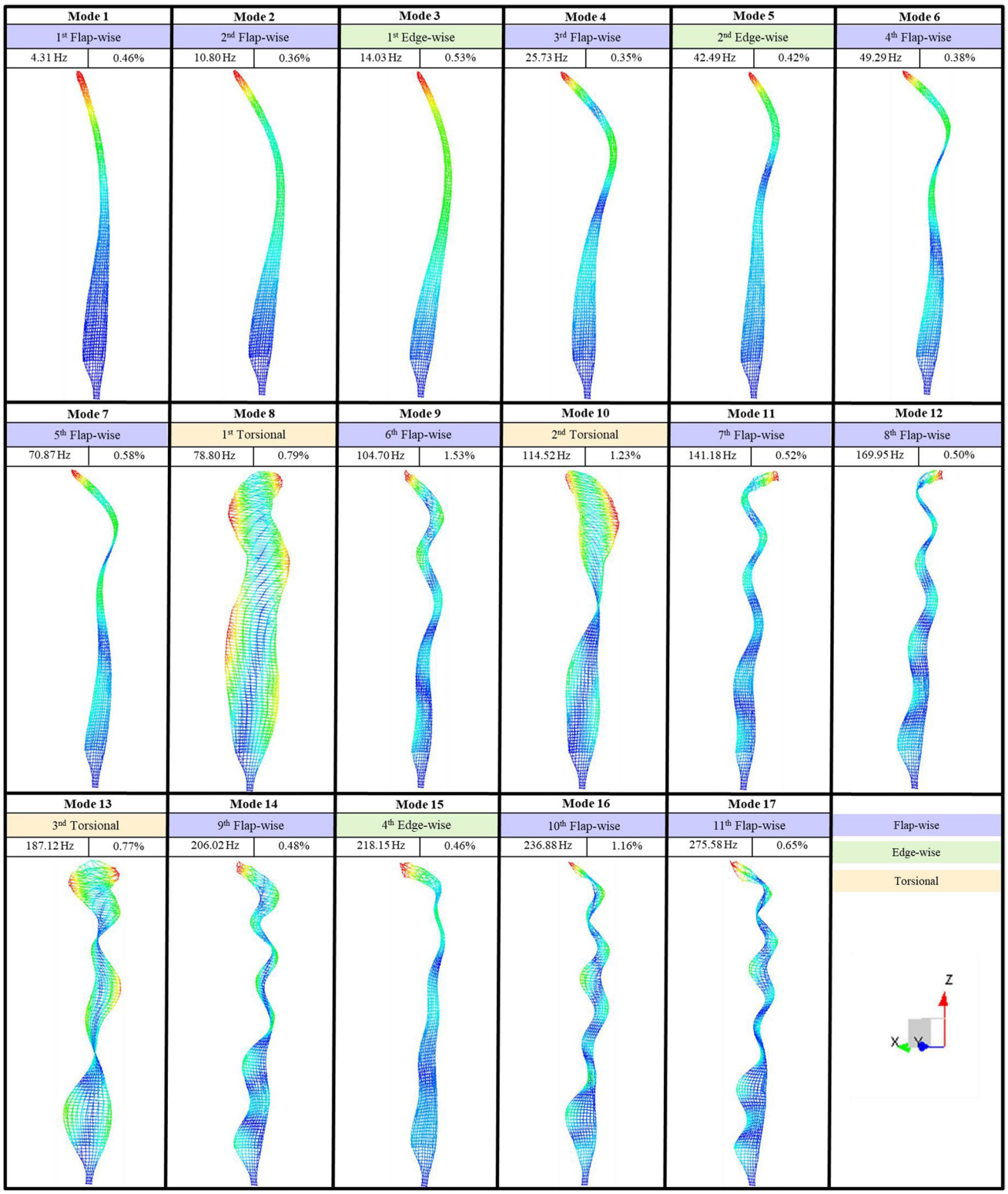

Fig. 13 Modal Parameters of the Stitched Surface 1&2

surfaces should also be the same. This is also to validate the consistency of the measurement of Surface 1 and Surface 2. But, the two surfaces don't share any scan points, and there are no scan points that locate on both surfaces. However, the force input and acceleration response at the impedance head of the shaker is measured when measuring the two surfaces, which is also called the drive point FRF. The drive point FRF measured from the two surfaces is

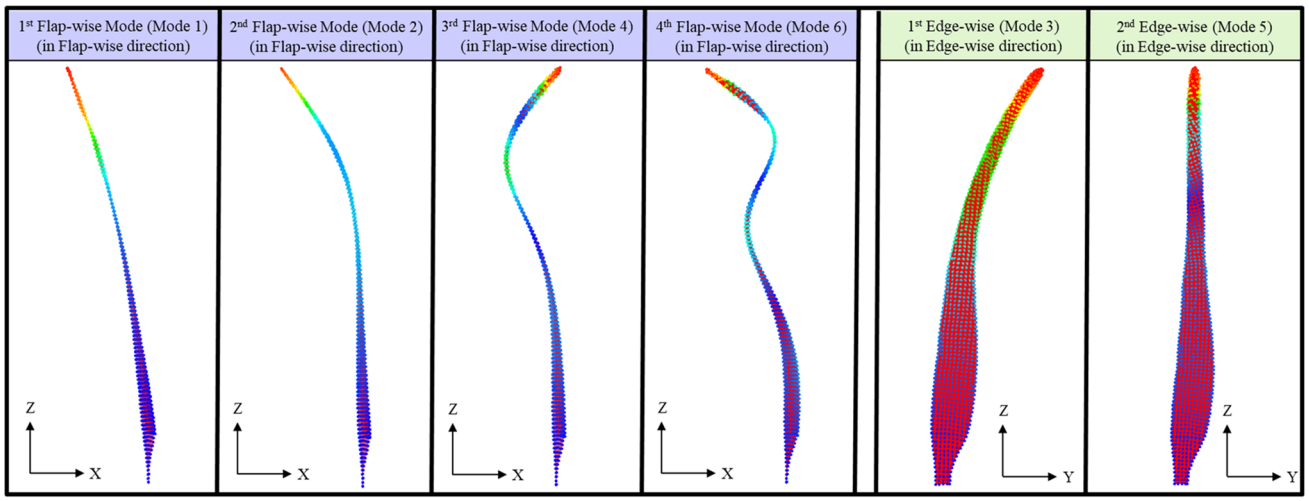

Fig. 14 Mode Shapes of the Stitched Surface 1&2 in Corresponding Main Plane

compared, as shown in Fig. 16. The drive point FRF measured from the Surface 1 has an excellent overlay with the drive point FRF measured from Surface 2 over the entire frequency band. This excellent agreement also shows the consistency of the measurement of the two surfaces.

Similarity of the Two Surfaces

AutoMAC is performed on the mode shapes of either Surface 1, Surface 2, or Stitched Surface 1&2 to check the orthogonality of the measured mode shapes to validate the measurement effectiveness. In Sect. 5.3, the mode shapes of Stitched Surface 1&2 are visually observed and compared. Generally, from observation of the mode shapes of Surface 1&2 in Fig. 13, Surface 1 and Surface 2 have a better match over the low-order modes than the high-order modes. This section quantifies the similarity of the two surfaces with the CrossMAC. CrossMAC is employed to correlate the mode shapes of Surface 1 with Surface 2 to check the similarity between the two surfaces. The diagonal terms of the CrossMAC table in Fig. 17 are of interest and quantify the mode shape comparison between the two surfaces. Each element of the diagonal terms of the CrossMAC table shows the MAC between the mode shape pair. Surface 1 and Surface 2 have over 90% similarity from Mode 1 to Mode 6, which shows that the measured mode shapes from the two surfaces are similar. Mode 7 to Mode 15 also have a correlation of over 70%, which also shows

90%-100%	70%-90%		Surface 1&2																
50%-70%	0-30%		Mode 1	Mode 2	Mode 3	Mode 4	Mode 5	Mode 6	Mode 7	Mode 8	Mode 9	Mode 10	Mode 11	Mode 12	Mode 13	Mode 14	Mode 15	Mode 16	Mode 17
		MAC	4.31 Hz	10.8 Hz	14.03 Hz	25.73 Hz	42.49 Hz	49.29 Hz	70.87 Hz	78.8 Hz	104.69 Hz	114.52 Hz	141.18 Hz	169.95 Hz	187.12 Hz	206.02 Hz	218.15 Hz	236.88 Hz	275.58 Hz
Surface 1&2	Mode 1	4.31 Hz	100%	5%	2%	2%	2%	1%	3%	0%	2%	0%	2%	2%	0%	1%	1%	1%	2%
	Mode 2	10.8 Hz	5%	100%	0%	9%	0%	3%	2%	1%	2%	0%	2%	2%	0%	2%	2%	1%	2%
	Mode 3	14.03 Hz	2%	0%	100%	1%	6%	0%	0%	1%	0%	0%	0%	1%	0%	1%	0%	1%	1%
	Mode 4	25.73 Hz	2%	9%	1%	100%	4%	9%	4%	0%	2%	0%	4%	4%	0%	3%	3%	1%	2%
	Mode 5	42.49 Hz	2%	0%	6%	4%	100%	3%	3%	1%	3%	0%	0%	2%	1%	1%	0%	2%	2%
	Mode 6	49.29 Hz	1%	3%	0%	9%	3%	100%	5%	2%	2%	0%	5%	2%	1%	1%	3%	1%	2%
	Mode 7	70.87 Hz	3%	2%	0%	4%	3%	5%	100%	1%	8%	0%	5%	4%	0%	2%	2%	2%	3%
	Mode 8	78.8 Hz	0%	1%	1%	0%	1%	2%	1%	100%	0%	6%	0%	1%	0%	0%	0%	1%	1%
	Mode 9	104.69 Hz	2%	2%	0%	2%	3%	2%	8%	0%	100%	1%	8%	4%	1%	4%	0%	1%	3%
	Mode 10	114.52 Hz	0%	0%	0%	0%	0%	0%	0%	6%	1%	100%	1%	0%	4%	0%	1%	0%	0%
	Mode 11	141.18 Hz	2%	2%	0%	4%	0%	5%	5%	0%	8%	1%	100%	10%	0%	1%	8%	3%	4%
	Mode 12	169.95 Hz	2%	2%	1%	4%	2%	2%	4%	1%	4%	0%	10%	100%	2%	9%	2%	2%	4%
	Mode 13	187.12 Hz	0%	0%	0%	0%	1%	1%	0%	0%	1%	4%	0%	2%	100%	0%	0%	6%	2%
	Mode 14	206.02 Hz	1%	2%	1%	3%	1%	1%	2%	0%	4%	0%	1%	9%	0%	100%	3%	2%	1%
	Mode 15	218.15 Hz	1%	2%	0%	3%	0%	3%	2%	0%	0%	1%	8%	2%	0%	3%	100%	1%	2%
	Mode 16	236.88 Hz	1%	1%	1%	1%	2%	1%	2%	1%	1%	0%	3%	2%	6%	2%	1%	100%	8%
	Mode 17	275.58 Hz	2%	2%	1%	2%	2%	2%	3%	1%	3%	0%	4%	4%	2%	1%	2%	8%	100%

Fig. 15 AutoMAC of the Mode Shapes of the Stitched Surface 1&2

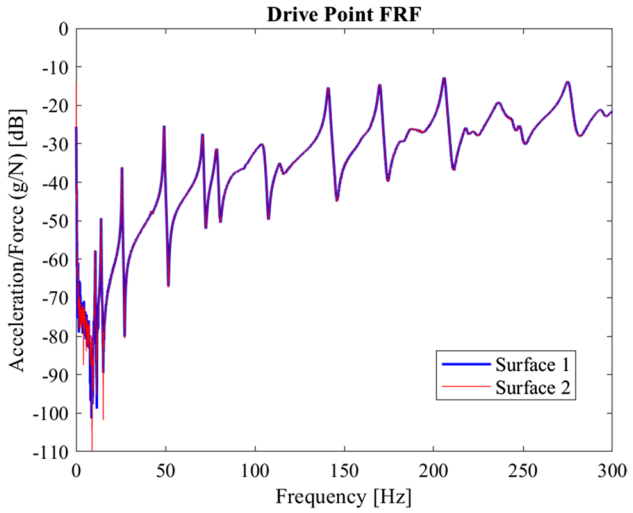

Fig. 16 Drive Point FRF Measured from the Two Surfaces

good similarity. Overall, the CrossMAC table quantitively indicates that the two surfaces have more similarity over the low-frequency range than the high-frequency range, which reflects the visual observation of the mode shapes of Surface 1&2 in Fig. 13.

Local Panel Mode

Panel modes are localized modes that are active in the blade panels [3, 4]. The panel modes are not global and appear in a relatively small region on the blade. If only a few sensors are available in the measurement, for example, blade instrumented with accelerometers, the panel modes cannot be identified from the sparse sensors. One of the advantages of the 3D SLDV is its capability of measuring a large volume of points in three directions. The 3D SLDV can provide a sufficient number of sensors to avoid spatial aliasing and capture the local panel modes. In addition, the panel modes usually appear in the high-frequency range. The 3D SLDV has a high-frequency range data acquisition capability, which can cover the high-order blade modes. This has great benefit to characterizing the blade local panel modes.

When closely examining mode shapes of Surface 1&2 in Fig. 13, three flap-wise modes have shown local panel modes, as identified in Fig. 18. The panel mode appears in the large panel sections of the blade. Both Surface 1 and Surface 2 provide the same indication of the panel modes. This is another merit of the two-surface measurement which is the cross-validation between the two surfaces. Having an understanding of the local panel modes can be useful for dynamic characterization and structural health monitoring of the blade panels [4].

To further show the benefit of the two-surface measurement, the panel mode, for example in Mode 14, is viewed separately by a cross-section at the blade span 1 m to the blade root, as shown in Fig. 19. The undeformed and deformed blades in two surfaces of this panel mode are plotted by plotting the cross-section of this mode shape at different points in the mode cycle: (1) at the positive peak (maximum relative motion of panels away from one another), (2) for the undeformed case, and (3) at the negative peak (smallest relative motion of panels toward one another). With the two surfaces' measurement capability, the relative deformation of the two surfaces can be characterized by a sufficient number of experimental sensors.

90%-100%	70%-90%		Surface 2															
50%-70%	0-30%		Mode 1	Mode 2	Mode 3	Mode 4	Mode 5	Mode 6	Mode 7	Mode 8	Mode 9	Mode 10	Mode 11	Mode 12	Mode 13	Mode 14	Mode 15	Mode 16	Mode 17
		MAC	4.31 Hz	10.8 Hz	14.03 Hz	25.73 Hz	42.49 Hz	49.28 Hz	70.87 Hz	78.79 Hz	104.68 Hz	114.47 Hz	141.17 Hz	169.92 Hz	186.99 Hz	205.99 Hz	218.12 Hz	236.73 Hz	275.54 Hz
Surface 1	Mode 1	4.31 Hz	100%	5%	2%	2%	1%	1%	3%	0%	2%	0%	3%	2%	2%	1%	1%	3%	3%
	Mode 2	10.8 Hz	4%	99%	0%	10%	0%	4%	1%	2%	2%	0%	3%	3%	0%	2%	3%	3%	4%
	Mode 3	14.03 Hz	2%	0%	99%	1%	6%	0%	0%	1%	0%	0%	0%	1%	0%	1%	0%	1%	1%
	Mode 4	25.74 Hz	2%	8%	1%	94%	1%	9%	4%	0%	2%	1%	3%	3%	1%	3%	3%	2%	2%
	Mode 5	42.5 Hz	1%	0%	6%	3%	95%	2%	2%	2%	3%	0%	0%	1%	1%	1%	0%	3%	2%
	Mode 6	49.29 Hz	1%	3%	0%	8%	0%	93%	4%	2%	1%	0%	5%	2%	0%	1%	4%	2%	3%
	Mode 7	70.87 Hz	3%	1%	0%	3%	3%	4%	87%	0%	6%	0%	3%	4%	0%	2%	2%	3%	4%
	Mode 8	78.81 Hz	1%	0%	1%	0%	1%	1%	0%	90%	0%	6%	0%	1%	0%	0%	1%	0%	1%
	Mode 9	104.73 Hz	3%	2%	1%	1%	1%	1%	5%	0%	83%	1%	7%	1%	1%	4%	1%	2%	3%
	Mode 10	114.55 Hz	2%	0%	0%	0%	0%	0%	1%	6%	1%	90%	1%	0%	4%	0%	1%	0%	0%
	Mode 11	141.19 Hz	2%	1%	0%	2%	0%	3%	2%	0%	3%	1%	76%	8%	0%	0%	6%	1%	2%
	Mode 12	169.97 Hz	2%	1%	1%	3%	0%	1%	2%	0%	2%	0%	4%	73%	4%	10%	1%	1%	2%
	Mode 13	187.28 Hz	0%	0%	0%	0%	1%	1%	0%	0%	0%	3%	0%	1%	81%	0%	0%	5%	1%
	Mode 14	206.05 Hz	1%	2%	1%	1%	1%	1%	0%	0%	2%	0%	1%	3%	0%	75%	2%	2%	0%
	Mode 15	218.17 Hz	1%	2%	0%	2%	0%	2%	1%	0%	0%	1%	5%	0%	0%	2%	83%	0%	0%
	Mode 16	236.98 Hz	0%	0%	0%	1%	1%	0%	2%	1%	0%	0%	2%	0%	1%	0%	0%	59%	6%
	Mode 17	275.66 Hz	1%	0%	0%	1%	1%	1%	1%	0%	2%	0%	1%	2%	1%	0%	0%	3%	51%

Fig. 17 CrossMAC of the Mode Shapes Between the Two Surfaces

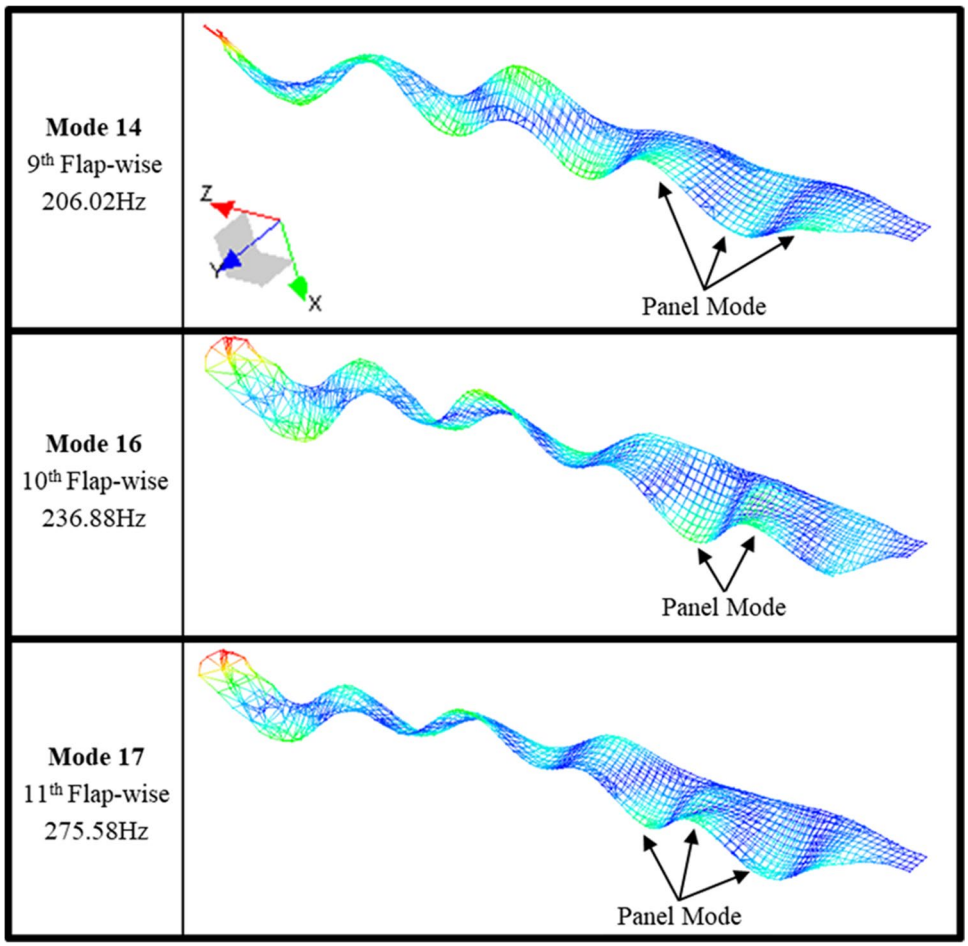

Fig. 18 Localized Panel Modes of Wind Turbine Blade

This example shows a great advantage of the proposed two surface measurement technique over the one surface measurement which would fail to represent the relative distortion of the two surfaces.

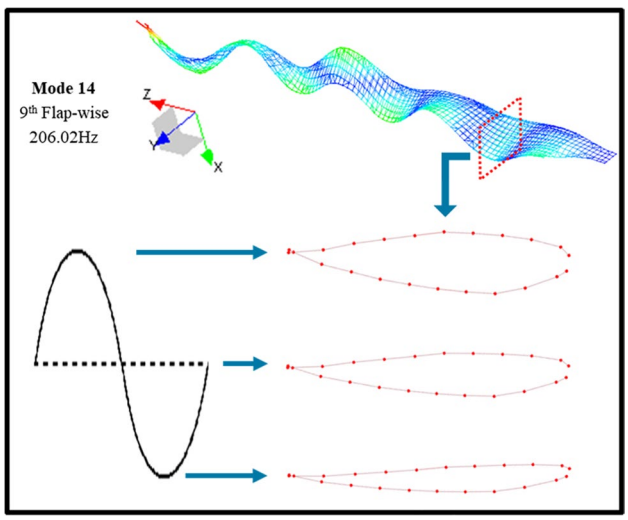

Fig. 19 Localized Panel Modes in Cross-Section

Conclusion

This work proposes a new method of measuring the mode shapes of both surfaces of the wind turbine blade. The methodology developed in this work could also benefit other 3D structures. Such two-surface modal testing is conducted on a wind turbine blade with a high spatial resolution 3D Scanning Laser Doppler Vibrometer (SLDV). The two surfaces of the wind turbine blade are scanned and measured by the 3D SLDV respectively under the same global test coordinate system defined by the alignment objects. The mode shapes of the Surface 1 and Surface 2 are stitched together to build the blade mode shapes of Surface 1&2. Flap-wise, edge-wise, and torsional mode shapes are obtained in a non-contact fashion from scanning 1,521 points (4,563 response DOF) on both surfaces of one blade. This high spatial resolution FRF measurement can easily capture the complex curvature mode shapes. All blade modes below 300 Hz are studied. The measured mode shapes of Surface 1, Surface 2, and Surface 1&2, are validated to be high orthogonality mode shape bases by the correlation tool, MAC. The drive point FRF measured from both surfaces is shown to have an excellent agreement to demonstrate the measurement

consistency between the two-surface measurement. Surface 1 and Surface 2 give close frequency and well-correlated mode shapes. With the high spatial resolution measurement capability of the 3D SLDV, several local panel modes of the wind turbine blade are identified. This work provides an in-depth understanding of the dynamics of wind turbine blades on both surfaces. The identified local panel modes would benefit us greatly to conduct structural and reliability analysis to find the root cause or failure mechanism for the operating wind turbine blade. This also provides blade designers with useful information about the blade modal properties that can be used while performing blade structural design, which is increasingly important as wind turbines grow larger to further reduce the cost of energy. Lastly, this work can provide a general technique for capturing the dynamics of shell or plate structures where the relative motion of shells is important to measure, characterize, and evaluate.

Acknowledgements The authors thank Kyle Wetzel from Wetzel Engineering Inc. for the donation of the 4.2-meter blade test articles to the University of Texas at Dallas and Viryd Technologies Inc. for having supported the design and development of the blades. The authors are also grateful to the University of Texas System and the University of Texas at Dallas for STARs award funding that supported this research.

Declarations

Competing Interests In accordance with Springer Nature Editorial Policy, it is reported that Yuanchang Chen serves as a Technical Editor for SEM Experimental Techniques.

References

1. Griffith DT, Ashwill TD (2011) The Sandia 100-meter all-glass baseline wind turbine blade: SNL100–00. Informe Técnico, Sandia National Laboratories
2. Jensen FM, Weaver PM, Cecchini LS, Stang H, Nielsen RF (2012) The Brazier effect in wind turbine blades and its influence on design. Wind Energy 15:319–333
3. Griffith DT, Paquette J (2010) Panel resonant behavior of wind turbine blades. In 51st AIAA/ASME/ASCE/AHS/ASC Structures, Structural Dynamics, and Materials Conference 18th AIAA/ASME/AHS Adaptive Structures Conference 12th, p 2741
4. Griffith DT (2011) Utilization of localized panel resonant behavior in wind turbine blades. In Proulx T (ed) Rotating machinery, structural health monitoring, shock and vibration, vol 5. Conference Proceedings of the Society for Experimental Mechanics Series. Springer, New York, NY. https://doi.org/10.1007/978-1-4419-9428-8_8
5. Griffith DT, Yoder NC, Resor B, White J, Paquette J (2014) Structural health and prognostics management for the enhancement of offshore wind turbine operations and maintenance strategies. Wind Energy 17:1737–1751
6. Myrent N, Adams DE, Griffith DT (2015) Wind turbine blade shear web disbond detection using rotor blade operational sensing and data analysis. Philos Trans R Soc A Math Phys Eng Sci 373:20140345
7. Chen X (2019) Experimental observation of fatigue degradation in a composite wind turbine blade. Compos Struct 212:547–551
8. Cao D, Malakooti S, Kulkarni VN et al (2022) The effect of resin uptake on the flexural properties of compression molded sandwich composites. Wind Energy 25(1):71–93. https://doi.org/10.1002/we.2661
9. Griffith DT, Carne TG, Paquette JA (2008) Modal testing for validation of blade models. Wind Eng 32:91–102
10. Chen Y, Logan P, Avitabile P et al (2019) Non-model based expansion from limited points to an augmented set of points using Chebyshev polynomials. Exp Tech 43:521–543. https://doi.org/10.1007/s40799-018-00300-0
11. Chen Y, Avitabile P, Dodson J (2020) Data Consistency Assessment Function (DCAF). Mech Syst Signal Process 141:106688
12. Chen Y, Avitabile P, Page C, Dodson J (2021) A polynomial based dynamic expansion and data consistency assessment and modification for cylindrical shell structures. Mech Syst Signal Process 154:107574
13. Lundstrom T, Baqersad J, Niezrecki C, Avitabile P (2012) Using high-speed stereophotogrammetry techniques to extract shape information from wind turbine/rotor operating data. In Allemang R, De Clerck J, Niezrecki C, Blough J (eds) Topics in modal analysis II, vol 6. Conference Proceedings of the Society for Experimental Mechanics Series. Springer, New York, NY. https://doi.org/10.1007/978-1-4614-2419-2_26
14. LeBlanc B, Niezrecki C, Avitabile P, Chen J, Sherwood J (2013) Damage detection and full surface characterization of a wind turbine blade using three-dimensional digital image correlation. Struct Health Monit 12:430–439
15. Baqersad J, Niezrecki C, Avitabile P (2015) Full-field dynamic strain prediction on a wind turbine using displacements of optical targets measured by stereophotogrammetry. Mech Syst Signal Process 62:284–295
16. Baqersad J, Niezrecki C, Avitabile P (2015) Extracting full-field dynamic strain on a wind turbine rotor subjected to arbitrary excitations using 3D point tracking and a modal expansion technique. J Sound Vib 352:16–29
17. Carr J, Baqersad J, Niezrecki C, Avitabile P (2016) Full-field dynamic strain on wind turbine blade using digital image correlation techniques and limited sets of measured data from photogrammetric targets. Exp Tech 40:819–831
18. Wu R, Zhang D, Yu Q, Jiang Y, Arola D (2019) Health monitoring of wind turbine blades in operation using three-dimensional digital image correlation. Mech Syst Signal Process 130:470–483
19. Khadka A, Fick B, Afshar A, Tavakoli M, Baqersad J (2020) Non-contact vibration monitoring of rotating wind turbines using a semi-autonomous UAV. Mech Syst Signal Process 138:106446
20. Luczak MM, Riva R, Yeniceli SC, Madsen SH, Di Lorenzo E (2021) Identification of the test setup influence on the modal properties of a short wind turbine blade during fatigue test. Measurement 174:108960
21. Chen Y, Escalera Mendoza AS, Griffith DT (2021) Experimental and numerical study of high-order complex curvature mode shape and mode coupling on a three-bladed wind turbine assembly. Mech Syst Signal Process 160:107873
22. Chen Y, Griffith DT (2021) Mode shape recognition of complicated spatial beam-type structures via polynomial shape function correlation. Exp Tech. https://doi.org/10.1007/s40799-021-00505-w
23. Chen Y, Todd Griffith D (2022) Finite cross-section method for mode shape recognition of highly coupled beam-type

structures. ASME J Vib Acoust 144(4):041013. https://doi.org/10.1115/1.4053977
24. Witt B, Rohe D, Schoenherr T (2019) Full-field strain shape estimation from 3D SLDV, Rotating Machinery, Optical Methods & Scanning LDV. Methods 6:31–45
25. Yuan K, Zhu W (2021) Modeling of welded joints in a pyramidal truss sandwich panel using beam and shell finite elements. ASME J Vib Acoust 143(4):041002. https://doi.org/10.1115/1.4048792
26. Polytec GmbH (2022) PSV-500-3D operating instructions manual
27. Rothberg SJ, Allen MS, Castellini P, Di Maio D, Dirckx JJJ, Ewins DJ, Halkon BJ, Muyshondt P, Paone N, Ryan T (2017) An international review of laser Doppler vibrometry: Making light work of vibration measurement. Opt Lasers Eng 99:11–22
28. Di Maio D, Castellini P, Martarelli M, Rothberg S, Allen MS, Zhu WD, Ewins DJ (2021) Continuous Scanning Laser Vibrometry: A raison d'être and applications to vibration measurements. Mech Syst Signal Process 156:107573
29. Chen Y, Joffre D, Avitabile P (2018) Underwater Dynamic Response at Limited Points Expanded to Full-Field Strain Response. J Vib Acoust 140:051016
30. Allemang RJ, Brown DL (1982) A correlation coefficient for modal vector analysis. In Proceedings of the 1st international modal analysis conference. SEM Orlando, pp 110–116
31. Chen Y, Griffith DT (2022) Experimental and numerical investigation of the structural dynamic characteristics for both surfaces of a wind turbine blade. J Vib Control. https://doi.org/10.1177/10775463221097470
32. Siemens AG (2022) Simcenter SCADAS mobile user manual